ISBN: 978-1-7281-0368-6 / IEEE Catalogue Number: CFP1948U-USB
http://doi.org/10.1109/RoboMech.2019.8704761

2019 SAUPEC/RobMech/PRASA Conference
Bloemfontein, South Africa, January 28-30, 2019

Design Strategy of Traction Induction Motors

T. M. Masuku, R-J. Wang*, M. C. Botha and S. Gerber
Dept. of Electrical and Electronic Engineering
Stellenbosch University
Stellenbosch, 7600
South Africa
Corresponding author: rwang@sun.ac.za*

***Abstract*—In this paper, a strategy for designing induction motors for traction applications is proposed. The proposed strategy builds on the conventional design of induction motors, but makes emphasis on the differentiating characteristics, which are the constant power speed ratio and overloading capability. A design procedure, which breaks up the motor design into different parts and phases was formulated. The formulated design strategy was then validated by the design of a 3 kW traction induction motor using the ANSYS Electronics packages. ANSYS RMxprt was used in conjunction with ANSYS Optimetrics optimization module to create an initial optimum design, which was then verified by using ANSYS Maxwell 2D finite element analysis. The proposed design strategy has been shown to work well.**

***Index Terms*—Design optimization, finite element analysis, induction motors, traction motors, flux weakening**

I. Introduction

Induction motors are widely used in traction applications because of their high efficiency, good overload capability and wide constant power speed range. The design strategy of an induction motor for traction applications is significantly different from that of the conventional induction motor [1]. For an induction motor to be deemed suitable for traction drives a set of requirements have to be met [2]–[4]: high power density, overload capability, high torque at low speeds, fast torque response, high reliability, high efficiency over wide torque and speed ranges, high durability and low cost. The aim of this paper is to formulate a design strategy that conforms to these requirements. The suggested approach will be implemented in the design of a traction induction machine.

A. Power and Torque Characteristics

The power and torque characteristics of a traction motor determine the vehicle's running performance, including the vehicle's acceleration, grade-ability and maximum speed [3], [4]. Typically, the output power and torque of a traction motor are broken down into three operating regions: constant torque, constant power and slip limited, as shown in Fig. 1.

In the constant torque region, the machine's rated torque is maintained by keeping a constant voltage-frequency ratio. This ratio maintains the flux level and the currents in the machine to the given rated values. The output power of the motor increases linearly with an increase of the supply voltage. The constant power region is entered when the supply frequency continues increasing while the voltage is at maximum breaking the constant voltage-frequency ratio. The machine current is constant but the air-gap flux reduces inversely to the supply frequency. This decreases the output torque inversely to the angular velocity and the output power remains constant. For the slip limited region the machine operates at breakdown slip to maximize the output torque, which results in the reduction of output power.

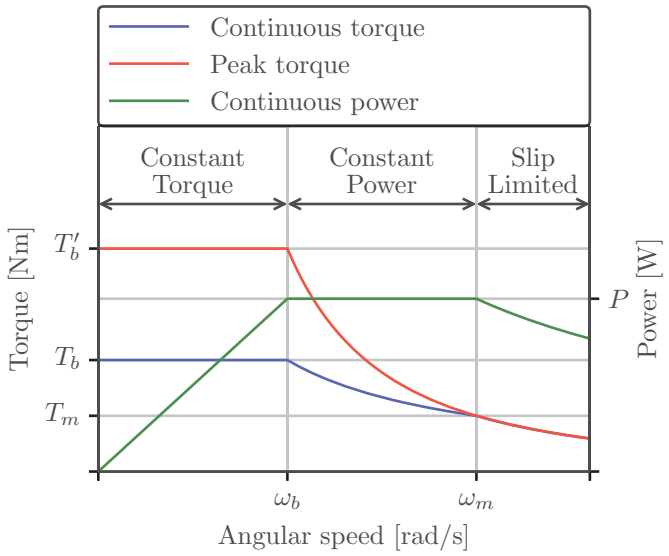

Fig. 1. Induction machine torque power characteristics [4]

B. Realizing Wide Constant Power Speed Range

For the design to be considered suitable for traction drives the Constant Power Speed Range (CPSR), which is defined as ω_m/ω_b as illustrated in Fig. 1, should be 3 or greater [3]. In other words, the maximum speed ω_m achieved in the constant power region should be a minimum of 3 times greater than the base speed ω_b. Since the design point is usually set at the base speed ω_b and the maximum constant power speed ω_m is a consequence thereof, it is essential to establish the relation between the two so that the design specifications at both speeds can be satisfied. Since the maximum torque of an $m-$phase, $p-$pole pair induction motor can be expressed as [3], [5]:

$$T' = \frac{p}{2\pi f} \cdot \frac{mV_{1eq}^2}{2\left(R_{1eq} + \sqrt{R_{1eq}^2 + (X_{1eq} + X_2)^2}\right)} \quad (1)$$

978-1-7281-0369-3/19/$31.00 ©2019 IEEE

where V_{1eq}, R_{1eq}, X_{1eq} and X_2 are equivalent stator voltage, resistances, leakage reactance and referred rotor leakage reactance, respectively.

Assuming R_{1eq} is negligible and V_{1eq} is constant under flux weakening operation, eqn. (1) can be written as:

$$T' = K \cdot \left(\frac{V_{1eq}}{f}\right)^2 \tag{2}$$

where $K = mp/[8\pi^2(L_{1eq}+L_2)]$ and L_{1eq} and L_2 are equivalent stator leakage and referred rotor leakage inductances.

Since $f \propto \omega$ (electrical angular speed) and V_{1eq} is constant:

$$T' \approx K_1 \frac{1}{\omega^2} \tag{3}$$

where K_1 is a constant. The relation between the maximum torques at the base and maximum speeds, ω_b and ω_m, is thus:

$$T'_b \cdot \omega_b^2 = T'_m \cdot \omega_m^2 \tag{4}$$

Under constant power P, the rated operational torques at the base and maximum speed, T_b and T_m, are related by:

$$P = \omega_b T_b = \omega_m T_m \tag{5}$$

At the maximum speed, the maximum torque must exceed the rated operating torque by a factor κ_m, such that:

$$T'_m = \kappa_m T_m \tag{6}$$

For example, in Fig. 1, $\kappa_m = 1$ and $T'_m = T_m$. From (4) – (6), the ratio between the maximum torque and the rated operational torque at the base speed, κ_b, can be derived:

$$T'_b = \kappa_b T_b \tag{7}$$

$$T'_b = \frac{\omega_m}{\omega_b}\kappa_m T_b \tag{8}$$

$$\implies \kappa_b = \frac{\omega_m}{\omega_b}\kappa_m \tag{9}$$

Eqn. (9) can be incorporated into the initial design steps to optimize a suitable maximum torque in order to realize the required CPSR for the induction motor.

C. Mitigation of Harmonic Losses

Traction induction motors are usually fed from voltage source inverters. The time harmonic content of the supply voltages cause additional copper and core losses resulting in high machine temperature. Often the motor rating has to be reduced somewhat to maintain the rated temperature [3], [6]. Another contributor for efficiency loss of a traction induction motor is the harmonic secondary copper losses in the rotor bars. These harmonic secondary copper losses occur in the conductor near the rotor surface and are produced by the harmonic component of the air-gap flux density due to the stator slots. To counter this problem and improve the efficiency of the traction induction motor, new rotor slot designs proposed in [7] as shown in Fig. 2 were considered. Taking the slot profile in Fig. 2A (A-type) as a base design, the configuration shown in Fig. 2B (B-type) involved only reducing the conductor size and without changing the slot shape. Although the results

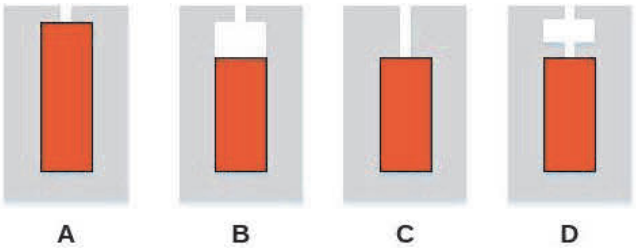

Fig. 2. Candidate rotor slot designs [7].

are promising, the conductor can shift from its position due to centrifugal force during operation. An alternative design as in Fig. 2C (C-type) is to place the conductor deeper in the rotor. Harmonic secondary copper losses are expected to reduce, however there is a chance that leakage inductance would increase in the upper portion of the rotor slots leading to reduced stalling torque. Fig. 2D (D-type) gives an interesting design, which was devised to withstand centrifugal forces as well as reduce the harmonic secondary copper losses without significantly increasing rotor leakage inductance.

II. Design Procedure

A. Design Specifications

The validation of the design procedure will be executed by the design of an induction motor with the following specifications:

TABLE I
KEY IM DESIGN SPECIFICATIONS

Description	Values
Rated power (kW)	3
Rated voltage (V)	380
Number of phases	3
Number of poles	4
Rated speed (rpm)	1000
Maximum speed (rpm)	3000
Overload ratio at maximum speed κ_m	≥ 1
Rated efficiency	$\geq 80\%$
Rated power factor	≥ 0.7
Winding configuration	Delta
Core material	M19-26Ga
Rotor bar material	Copper
Allowable stator outer diameter (mm)	190

In addition to these specifications, the motor should have ideal electric and magnetic loading values to avoid oversaturation and overheating.

B. Selection of Number of Slots

In an induction motor design, the selection of number of stator and rotor slots needs careful consideration. To reduce the leakage reactance, the number of stator slots per pole per phase should generally greater than two [8]. For a 4-pole small induction motor, 24/36/48 slots can be viable options.

In order to avoid disturbances in the operation of an induction motor, the rotor slots have to be carefully selected with respect to the stator slots. Common problems which arise

due to the incorrect selection of rotor and stator slot number combinations are cogging and crawling defined as follows:

- *Cogging:* Also known as *magnetic locking*, is when the motor refuses to start up and remains stationary. This normally occurs when the number of stator slots equal the number of rotor slots. When the rotor and stator slots face each other, the reluctance of the magnetic path is minimum so the rotor position tends to remain fixed [9], [10].
- *Crawling:* The rotating magnetic field in the air-gap of the motor is normally non-sinusoidal and generally contains odd harmonics of the 3^{rd}, 5^{th} and 7^{th} order. The presence of harmonics in the flux wave affects the torque speed characteristics. A motor with a presence of 7^{th} order harmonics will have a tendency to run at one seventh of its normal speed [9], [10].

The following guidelines can be used in conjunction with Fig. 3 to better define the selection of rotor slots:

- To avoid cogging and crawling $Q_s \neq Q_r$ and $(Q_s - Q_r) \neq \pm 3p$
- To avoid synchronous hooks and cusps in torque speed characteristics $Q_r \neq \pm p, \pm 2p, \pm 5p$
- To avoid noisy operation $(Q_s - Q_r) \neq \pm 1, \pm 2, (\pm p \pm 1), (\pm p \pm 2)$

The combinations without symbols shown in Fig. 3 are safe choices. For the 3 kW IM design, the number of slots for stator and rotor are chosen as 36 and 30, respectively.

		Number of pole pairs $p = 1$										Number of pole pairs $p = 2$									
	Tens of rotor	Ones of rotor slot number Q_r										Ones of rotor slot number Q_r									
Q_s	slot number	0	1	2	3	4	5	6	7	8	9	0	1	2	3	4	5	6	7	8	9
24	1	−	×	○	×	+	×	−	×	○	×	−	×	○	×	+	×	+	×		×
	2	+	×	−	×	○	×	+	×	−	×	−	×	−	×	○	×	+	×	+	×
	3	○	×	+	×	−	×	○	×	+	×		×	−	×		×	○	×		×
36	1	−	×	○	×	+	×	−	×	○	×		×	○	×		×	∓	×	○	×
	2	+	×	−	×	○	×	+	×	−	×	±	×		×	○	×		×	+	×
	3	○	×	+	×	−	×	○	×	+	×		×	−	×	−	×	○	×	+	×
	4	−	×	○	×	+	×	−	×	○	×	+	×		×	−	×		×	○	×
	5	+	×	−	×	○	×	+	×	−	×		×	+	×		×	−	×		×
48	1	−	×	○	×	+	×	−	×	○	×		×	○	×		×	+	×		×
	2	+	×	−	×	○	×	+	×	−	×	−	×	−	×	○	×	+	×	+	×
	3	○	×	+	×	−	×	○	×	+	×		×	−	×		×	○	×		×
	4	−	×	○	×	+	×	−	×	○	×	+	×		×	−	×	−	×	○	×
	5	+	×	−	×	○	×	+	×	−	×	+	×	+	×		×	−	×		×
	6	○	×	+	×	−	×	○	×	+	×	○	×		×	+	×		×	−	×

Fig. 3. Rotor and stator slot safe combinations [10], where "−" stands for harmful torques in counter-current braking, "+" stands for harmful torques at positive speeds, "×" represents harmful mechanical vibrations, and "○" refers to harmful synchronous torques at standstill.

C. Design Steps

Fig. 4 shows a high level flow diagram of the complete design procedure.

- Step 1: Selection of the initial diameter and core lengths based on sizing equation.
- Step 2: The design of the stator, which includes selection of the number of slots and winding types.
- Step 3: The design of the rotor, which includes the selection of the number of rotor slots, rotor slot type, air-gap length and the rotor shaft diameter.
- Step 4: The performance evaluation of the initial design is conducted, which includes efficiency, power factor, torque-speed curve during flux weakening, magnetic loading, electric loading etc.
- Step 5: The optimization of the design.
- Step 6: If the optimization results are the desired characteristics then proceed to Step 7. Otherwise it will loop back into Step 5 after redesigning the constraints.
- Step 7: Finite Element Analysis of the analytical design is conducted.
- Step 8: If the results are validated in all cases the design can proceed to Step 9. Otherwise it will loop back to Step 5, to re-design and re-optimize the motor.
- Step 9: The final optimized and verified design can be manufactured. The electromagnetic design process is complete.

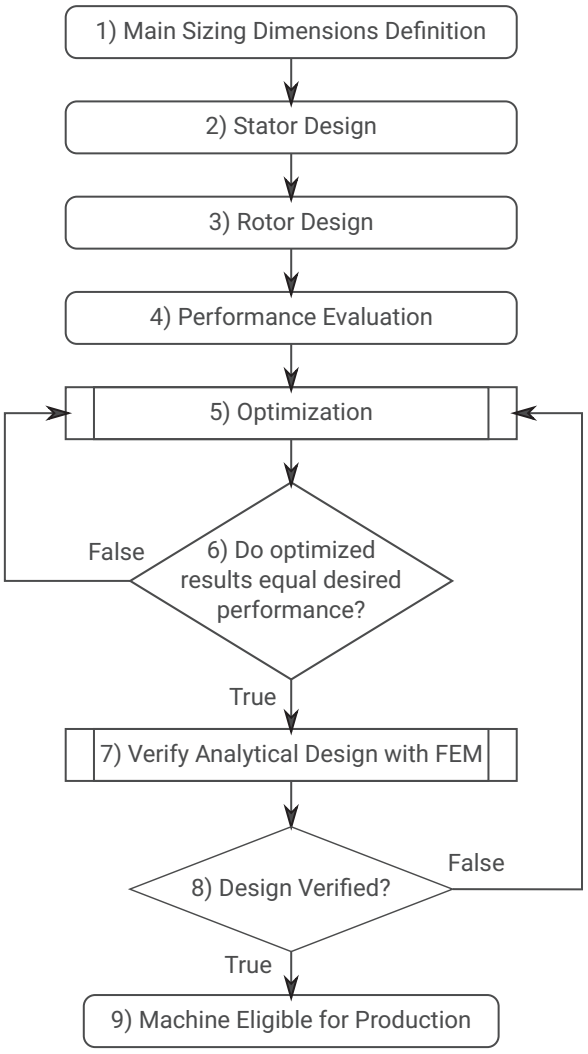

Fig. 4. Design flow diagram.

The optimization of the design, conducted in step 5, can generally be approached in several different ways. Different types of optimization algorithms may be employed. Further-

more, there are many different ways in which the optimization problem may be formulated, depending on the specific requirements of the application, the capabilities of the analysis function and the nature of the optimization algorithm.

In this study, the optimization was conducted using RMxprt analyses together with ANSYS' built-in optimization tool. The genetic algorithm was employed. Using these tools, the optimization problem was formulated as an unconstrained problem:

$$\text{Minimize:} \quad F(\mathbf{X}) = \sum_i [w_i G_i(X)] \tag{10}$$

where F is the objective function, X is the set of design variables, w_i is a set of weighting functions and G_i is a set of penalty functions for constraints. The constraints considered in this process were:

$$\eta \geq 80\,\% \tag{11}$$
$$\text{PF} \geq 70\,\% \tag{12}$$
$$P_{\text{out}} = 3\,\text{kW} \tag{13}$$
$$T_b' \geq 100\,\text{Nm} \tag{14}$$

where η is the efficiency, PF is the power factor, P_{out} is the rated continuous output power and T_b' is the breakdown torque. The weighting functions in (10) were all chosen as unity.

III. Analysis of Results

To verify the traction induction motor design strategy, results of both the analytical design model and finite element analysis are compared. Table I shows the design specifications of the traction induction motor, which is to be modeled and validated. In addition, a stator outer diameter constraint of 190 mm is put in place to limit the size of the machine to standard frame sizes. Although better performance can be expected with a bigger size machine the results summarized in this section are within reasonable margins.

The analytical design cross section is shown in Fig. 5a. The experimental rotor slot profile discussed in Section I-C is implemented in 2D Maxwell using the draw tool and is shown in Fig. 5b.

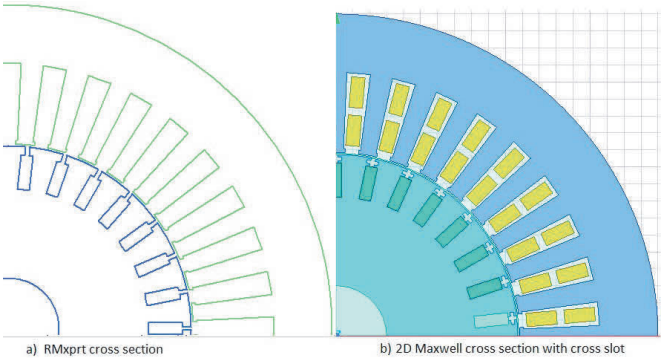

Fig. 5. The cross-sections of the optimum induction motor: (a) with C-type rotor slots, and (b) with D-type rotor slots.

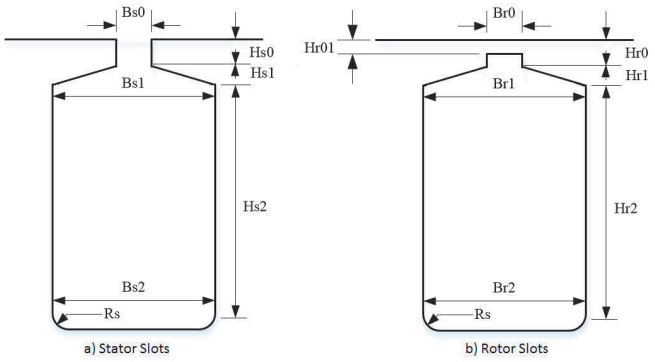

Fig. 6. Definition of slot dimensions for (a) stator slots, and (b) rotor slots.

The optimized slot and sizing dimensions of the machine are summarized in Table II with their definitions shown in Fig 6. The rated performance is summarized on Table III together with the calculated circuit parameters. These results are obtained from the analytical model (RMxprt) and need to be verified by using more accurate numeric modeling method like Finite Element Method (FEM).

TABLE II
Induction Motor Optimized Dimensions

Stator (36 slots)	Initial [mm]	Optimum [mm]
Hs0	0.8	1
Hs1	0	0
Hs2	28	22.5
Bs0	5	4
Bs1	6	5
Bs2	8.5	7
Rs	0	0
Rotor (30 slots)	**Initial [mm]**	**Optimum [mm]**
Hr0	5	2.5
Hr1	0	0
Hr2	15	10
Br0	2.5	1.2
Br1	5.5	3.5
Br2	5.5	3.5
Hr01	0	0
Rs	0	0
General	**Initial [mm]**	**Optimum [mm]**
Core length	105	160
Outer diameter	220	190
Inner diameter	120	108
Shaft diameter	40	30
Air-gap length	0.3	0.65

A. Performance Characteristics

The torque-speed characteristics of the designed traction induction motor obtained using ANSYS analytical design tool RMxprt is shown in Fig. 7. The corresponding power-speed curve is given in Fig. 8, which shows a constant power speed range close to 3. For validation purpose, ANSYS Maxwell 2D FEM is used to compute the output power at both base speed and maximum speed points. The 2D Maxwell results shown in Fig. 9 gives an output power of 3010 W at 1000 rpm and 2949 W at 3000 rpm, which is in a good agreement with that

TABLE III
RATED PERFORMANCE OF THE OPTIMUM INDUCTION MOTOR

Performance parameters	Values	Units
Input power	3558,14	W
Total losses	558,085	W
Output power	3000	W
Rated efficiency	84.31%	-
Power factor	0.712	-
Rated torque	28.6	Nm
Rated speed	1000.29	rpm
Rated slip	0.0383	-
Source frequency	34.67	Hz
Calculated circuit parameters	Values	Units
Stator resistance (R_s)	1.979	Ω
Rotor resistance (R_r)	1.567	Ω
Stator leakage reactance (X_{ls})	1.495	Ω
Rotor leakage reactance (X_{lr})	2.752	Ω
Magnetizing reactance (X_m)	40.249	Ω
Core loss resistance (R_c)	2356.890	Ω

of RMxprt. The power at the maximum speed is slightly less than the specified 3 kW.

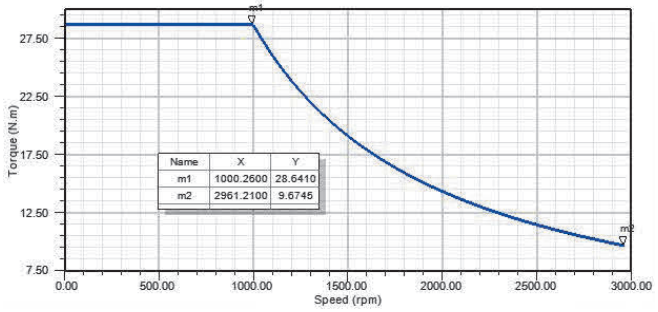

Fig. 7. Torque-speed characteristics of the optimum induction motor design obtained from RMxprt.

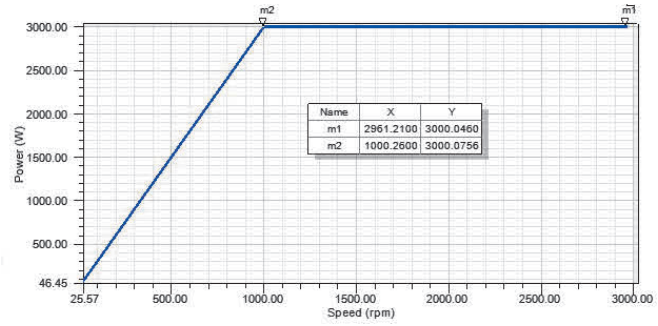

Fig. 8. Power-speed characteristics of the optimum induction motor design obtained from RMxprt.

B. Magnetic and Electric Loading

In a well designed induction machine, the highest flux density occurs in the teeth. As a further review of the design, the average magnetic and electric loadings obtained in the ANSYS RMxprt analytical design are summarized on Table IV together with the recommended value range set out as design guidance in [3], [11]. Generally, the design values correspond to desired characteristics and show a quality design.

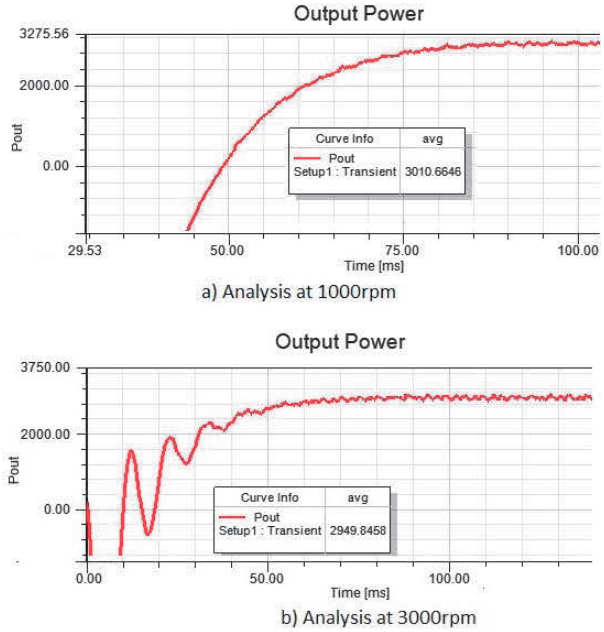

Fig. 9. Transient power analysis using 2D Maxwell.

TABLE IV
MAGNETIC AND ELECTRIC LOADING

Flux density (T)	Design value	Recommended values
Stator teeth	1.375	1.4 - 1.7
Rotor teeth	1.503	1.5 - 1.8
Stator yoke	1.306	1.4 - 1.7
Rotor yoke	0.545	1.0 - 1.6
Air-gap	0.767	0.7 - 0.9
Current density (A/mm^2)		
Stator slot	6.470	5.0 - 6.5
Rotor bar	5.817	5.5 - 7.5

C. Harmonic Loss Reduction Analysis

The rotor slot types (A and D) shown in Fig. 2 were simulated using FEM in order to compare their harmonic secondary copper losses. The simulation involved modeling the exact same machine with the only difference being the rotor slots and simultaneously running them at synchronous speed to mimic true no-load conditions. The results of the experiment are summarized on Fig. 10. At 1000 rpm, the rotor eddy current loss and core loss in the machine with A-type rotor slots were 3.77 W and 29.53 W, respectively. For the D-type rotor slots, the eddy current loss and core loss were 0.00115 W and 29.72 W. This shows the effectiveness of reducing the secondary rotor eddy current losses just from altering the rotor slot. The core losses for both slot types are practically the same.

IV. MECHANICAL DESIGN

The mechanical design of the induction traction motor prototype is described in this section. Fig. 11 depicts a 3D model of the 3 kW induction motor created in AutoCad Inventor. For enhanced heat transfer, the model was designed as a frameless machine with a finned core outer surface. Each fin was

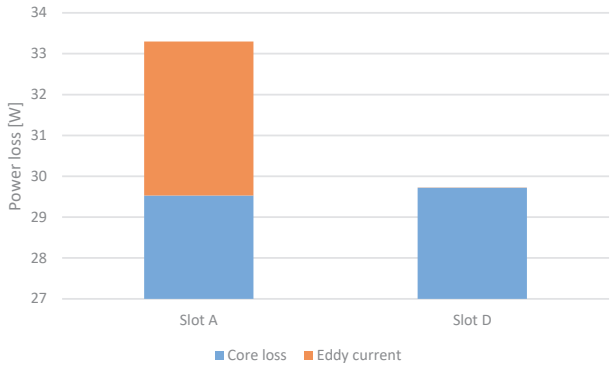

Fig. 10. Slot A and slot D loss comparison

designed with a heat transfer efficiency of 99 %. With 64 evenly distributed fins, a fin effectiveness of 3.34 was achieved. A detailed view of the fin dimensions can be seen in Fig. 12. With a winding temperature of 120 °C, ambient temperature at 40 °C and an assumed convective heat transfer coefficient of $h = 10$ W/m^{2}K, the rate of heat transfer from the induction machine was estimated as 189 W, which means that forced air cooling will be required.

The core consists of eight slots tangent to the outer surface of the stator as seen in Fig. 12. Manufacturing costs were further reduced by the inclusion of the rectangular cutaway for continuous laser cutting motion. The stator core laminations are compressed between two inner end-plates via four threaded rod and nut assemblies. Its further held stationary between two outer end-plates via four threaded rod, nut and bush assemblies. The bushing additionally serves as a spacer between the core and outer end-plate for winding purposes. The rotor is press-fitted onto the shaft and locked via a keyway and two circlips. A countersunk hole was created for each bushing on each outer end-plate for an embedded fit. Thus, increasing the overall rigidity of the machine.

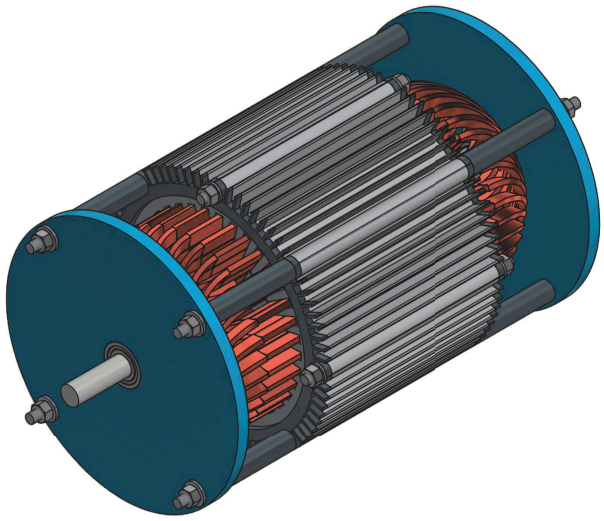

Fig. 11. 3D model of the designed 3 kW traction induction machine.

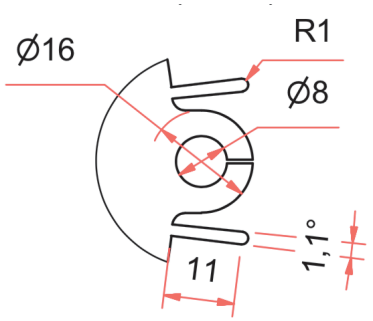

Fig. 12. Detailed view of finned lamination

V. Conclusion

The primary objective of formulating a design strategy for traction induction motors was met. Literature research on the motor technology was conducted and a high level flow diagram was created to summarize the applied design approach. Validation of the design approach was conducted using RMxprt and 2D FEM, which shows that the optimized traction motor has a good efficiency (84%) and power factor (0.71) even though a physical dimension restriction was put in place on the outer diameter. The designed induction traction motor had a CPSR of approximately 3 and the magnetic and electric loadings were within the desired ranges. These results give proof that the designed machine using the formulated approach is suitable for traction drive systems.

Acknowledgment

This work was supported in part by the Eskom Tertiary Education Support Program (TESP), National Research Foundation (NRF) and Stellenbosch University, all of South Africa.

References

[1] J. H. Lee, J. W. Kim, and Y. H. Kim, "Optimum design criteria for premium performance of traction induction motor," in *9th IET International Conference on Computation in Electromagnetics (CEM 2014)*, March 2014, pp. 1–2.

[2] J. F. Gieras and N. Bianchi, "Electric motors for light traction," *EPE Journal*, vol. 14, pp. 12–23, 2004.

[3] I. Boldea and S. Nasar, *The Induction Machines Design Handbook*. CRC Press, 2009.

[4] N. Zhao and N. Schofield, "An improved induction machine design procedure for electric vehicle traction," in *8th IET International Conference on Power Electronics, Machines and Drives (PEMD 2016)*, April 2016, pp. 1–6.

[5] C. Kingsley and S. D. Umans, *Fitzgerald and Kingsley's Electric Machinery*. McGraw Hill, 2003.

[6] P. K. Sen and H. Landa, "Derating of induction motors due to waveform distortion," *IEEE Transactions on Industry Applications*, vol. 26, no. 6, pp. 1102–1107, 1990.

[7] M. Kondo, M. Miyabe, and R. Ebizuka, "Design and efficiency evaluation of a high-efficiency induction motor for railway traction," *Electrical Engineering in Japanl*, vol. 194, no. 2, pp. 15–23, 2016.

[8] V. Mittle, *Design of Electrical Machines*. Standard Publishers Distributors, 2005.

[9] T. Lipo, *Introduction to AC machine design*. Wiley, 2017.

[10] J. Pyrhonen, T. Jokinen, and V. Hrabovcova, *Design of rotating electrical machines*, 2nd ed. Wiley, 2014.

[11] R. G. Harley and Y. Duan, "Traditional design of cage rotor induction motors," Grainger CEME, Seminars, 2009.